Korean Journal of Chemical Engineering
https://doi.org/10.1007/s11814-025-00638-3

ORIGINAL ARTICLE

Combined Effects of Alkaline Groundwater and Gamma Irradiation on the Durability of Geopolymer Waste Forms

Seongye Kwon[1] · Yulim Lee[1] · Yujin Oh[1] · Jaeyeong Park[1]

Received: 7 November 2025 / Revised: 18 December 2025 / Accepted: 29 December 2025

Abstract
The long-term durability of metakaolin (MK)-based geopolymer waste forms was evaluated under simulated disposal environments. Specimens incorporating Cs, Sr, and Co were fabricated and subjected to ANSI/ANS 16.1 leaching tests in deionized water (DI), concrete-saturated groundwater (CGW), and CGW combined with gamma irradiation (CGW+γ). Compressive strength, leachability index (LI), microstructure, and surface chemistry were analyzed to evaluate mechanical and chemical stability. All specimens initially satisfied the disposal acceptance criterion (≥3.45 MPa). The compressive strength remained stable in DI but declined under CGW due to alkali-induced degradation. Under the CGW+γ condition, severe strength loss occurred, and several specimens fractured completely. Leaching tests revealed substantial LI reduction for Cs, Sr, and Co. Computed tomography imaging showed increased porosity under CGW+γ, while X-ray photoelectron spectroscopy analysis confirmed Cs and Sr surface enrichment with the reduction of Co^{3+} to Co^{2+}. These results indicate that while MK-based geopolymers demonstrated strong resistance to individual degradation factors, they experienced significant structural deterioration under combined alkaline and radiation conditions, providing critical insights for the safe disposal of radioactive wastes.

Keywords Geopolymer waste form · Radionuclide immobilization · Leaching behavior · Gamma irradiation

Introduction

Safe disposal of radioactive waste requires solidification technologies capable of ensuring long-term stability. Geopolymers—alkali-activated, three-dimensional (3D) aluminosilicate gel network (K–A–S–H)—have attracted significant attention as next-generation waste forms due to their excellent chemical durability, low radionuclide leachability, and broad applicability to diverse waste streams [1–10]. Compared with Portland cement-based waste forms, geopolymers exhibit lower sensitivity to waste composition and greater tolerance for heavy metals and sulfides, further enhancing their potential [11–19].

However, degradation in actual disposal environments does not result from a single factor [20–22]. Instead, multiple stressors—such as strongly alkaline cementitious groundwater and radiation exposure—act simultaneously. Under such coupled conditions, alkali-induced dissolution of the Si–O–Al network can be intensified by radiolysis-driven acidification and bond cleavage, leading to mechanical weakening and accelerated radionuclide release [23–26]. Radiolysis generates reactive species (e.g., H·, ·OH, and H_2O_2) that locally modify redox conditions and disrupt charge balance within aluminosilicate frameworks, potentially altering cation binding environments. Such radiation-induced structural and chemical modifications have been experimentally observed in metakaolin-based geopolymers exposed to γ-irradiation, leading to measurable changes in mechanical and microstructural properties [27]. Despite these well-recognized degradation pathways, most previous studies have evaluated only isolated stressors—for example, leaching in benign aqueous environments, or mechanical testing after γ-irradiation. Systematic investigations addressing the simultaneous effects of alkalinity, ion exchange, microstructural depolymerization, and radiation-induced chemical alteration remain scarce. Moreover, prior research rarely investigated how these coupled degradation

✉ Jaeyeong Park
jypark@unist.ac.kr

[1] Department of Nuclear Engineering, Ulsan National Institute of Science and Technology, 50 UNIST-gil, Ulsan 44919, Republic of Korea

Published online: 23 January 2026

mechanisms influence element-specific bonding environments at the molecular scale, particularly through techniques such as X-ray photoelectron spectroscopy (XPS). As a result, the long-term stability of geopolymers under realistic, multi-stressor disposal conditions remains insufficiently understood [4, 26–41].

To address these knowledge gaps, this study focuses on a metakaolin (MK)-based geopolymer system activated with potassium hydroxide (KOH), selected as a representative and well-defined alkali-activated aluminosilicate matrix relevant to near-surface disposal environments. Cesium (Cs), strontium (Sr), and cobalt (Co) were chosen as target radionuclides because they represent distinct chemical classes critical to disposal safety assessments: monovalent alkali metals with high mobility (Cs), alkaline earth elements capable of Ca substitution (Sr), and redox-sensitive transition metals (Co). This study provides the first integrated assessment of MK-based geopolymer waste forms containing Cs, Sr, and Co under simultaneous chemical and radiation stress. Samples were subjected to three conditions: deionized water (DI), concrete-saturated groundwater (CGW), and CGW combined with gamma irradiation (CGW+γ). Their compressive strength, leachability index (LI), porosity (via computed tomography (CT) analysis), and surface chemistry (via X-ray photoelectron spectroscopy (XPS)) were comprehensively assessed. By explicitly linking macroscopic degradation indicators with XPS-derived changes in binding energy and oxidation state, this work provides new mechanistic insight into radiolysis-driven, element-specific destabilization processes that cannot be captured by bulk performance metrics alone.

Materials and Methods

Materials

MK was used as the primary aluminosilicate precursor for synthesizing the geopolymer waste forms. MK provides high purity, homogeneous composition, and excellent reactivity after calcination, with fewer impurities than fly ash or slag, thereby enabling more reproducible geopolymerization. Kaolin ($Al_2Si_2O_5(OH)_4$; CAS No. 1332-58-7, Sigma-Aldrich, USA) was calcined at 750 °C for 4 h to produce MK ($Al_2Si_2O_7$) [42]. Dehydroxylation of kaolinite occurs most efficiently between 600 and 800 °C, and the selected calcination condition ensured complete transformation to a reactive amorphous phase. The chemical composition of the calcined MK was characterized using X-ray fluorescence (XRF), and the results are summarized in Table 1.

KOH was used as the alkali activator. Although sodium hydroxide (NaOH) and potassium hydroxide (KOH) are widely used in geopolymer synthesis, their distinct cationic properties influence gel structure and long-term durability. The larger ionic radius and lower charge density of K^+ relative to Na^+ reduce structural constraint, favoring the formation of K–A–S–H gels with improved chemical stability.

The alkaline activator solution was prepared by dissolving KOH (45 wt%; CAS No. 1310-58-3, Sigma-Aldrich) in DI, followed by the addition of fumed silica (FS; particle size 0.2–0.3 μm, CAS No. 112945-52-5, Sigma-Aldrich). DI water was produced using a Mega Plus I ultrapure system (18.1 MΩ·cm). The final activator contained 16.74 wt% KOH and 5.06 wt% DI water. The solution was homogenized by shaking at 50 rpm for 12 h at room temperature (20 °C).

Design of Geopolymer Waste Forms

Geopolymer waste forms were fabricated with surrogate cationic radionuclides (Cs^+, Sr^{2+}, and Co^{2+}) at two concentrations (0.1 and 1 mmol). The molar ratios during synthesis were fixed at Si/Al = 1.8, K/Al = 1.0, and H_2O/Al = 1.0. These ratios were selected based on previous studies demonstrating that they promote the stable formation of geopolymer gels, ensure sufficient alkali activation, and maintain satisfactory workability during the fabrication process [43–46].

The target radionuclide concentrations were set to 10^{-3} mol and 10^{-4} mol per specimen, representing relatively low and high surrogate concentrations relevant to disposal scenarios. These loadings also enable reliable quantification using inductively coupled plasma mass spectrometry (ICP-MS) and inductively coupled plasma optical emission spectrometry (ICP-OES). Comparable surrogate concentrations have been widely adopted in previous geopolymer immobilization studies, allowing direct comparison with existing data [47]. $CsNO_3$, $Sr(NO_3)_2$, and $Co(NO_3)_2{\cdot}6H_2O$ were used as precursor salts to simulate actual radionuclides owing to their high aqueous solubility, which enables homogeneous mixing, and their suitability as non-radioactive analogs of the corresponding radionuclides.

These precursors were dissolved in DI before mixing with the geopolymer paste to ensure uniform dispersion. Duplicate specimens were prepared for each surrogate and experimental condition.

Table 1 Chemical composition of MK (XRF, wt%)

	SiO_2	Al_2O_3	Na_2O	K_2O	CaO	TiO_2	Fe_2O_3	P_2O_5
MK	50.8	46.5	0.07	0.17	0.04	1.41	0.77	0.10

Table 2 Geopolymer specimen types and surrogate radionuclides

Specimen type	Chemical form	Concentration (mmol)
Cs-1 mmol	$CsNO_3$	1.0
Cs-0.1 mmol	$CsNO_3$	0.1
Sr-1 mmol	$Sr(NO_3)_2$	1.0
Sr-0.1 mmol	$Sr(NO_3)_2$	0.1
Co-1 mmol	$Co(NO_3)_2{\cdot}6H_2O$	1.0
Co-0.1 mmol	$Co(NO_3)_2{\cdot}6H_2O$	0.1

Each geopolymer mixture was first stirred at room temperature for 5 min using a vortex mixer (Fisher Vortex Genie 2, Fisher Scientific, USA). The precursor powders and alkaline activator solution were then homogenized in a centrifugal mixer (ARE-310, THINKY, Japan) at 1,000 rpm for 90 s, followed by additional mixing at 1,200 rpm for 30 s to remove entrapped air bubbles. The resulting geopolymer paste was cast into cylindrical silicone molds (2 cm in diameter and 4 cm in height) and vibrated for 15 min to eliminate residual voids. All specimens were cured under ambient laboratory conditions (25 ± 1 °C) for 14 d prior to testing (Table 2).

Leaching Test

The leaching behavior of the geopolymer waste forms was evaluated following the ANSI/ANS 16.1 standard procedure. CGW was employed as the leachant to simulate the highly alkaline environment of radioactive waste repositories. CGW (pH ≥ 12.55) was prepared by equilibrating synthesized groundwater (SGW) with ordinary Portland cement (OPC) powder. The composition of SGW was formulated based on ion chromatography analyses of groundwater collected near the Gyeongju low- and intermediate-level radioactive waste repository site.

For SGW preparation, stock solutions of NaCl, $NaHCO_3$, Na_2SO_4, KCl, $CaCl_2$, $Ca(NO_3)_2$, and $MgCl_2$ were prepared at 100-fold the target concentrations and then mixed. In total 20 mL of the mixed stock solution was diluted with 1.86 L of DI water to obtain 2 L of SGW. CGW was prepared by adding 150 g of OPC powder to SGW and equilibrating the mixture. The major ionic compositions of SGW and CGW are summarized in Table 3.

N.D. = not detected.

As shown in Table 3, the concentrations of K^+ and Ca^{2+} increased significantly in CGW compared with SGW, consistent with the dissolution of cement hydration products such as $Ca(OH)_2$ and K_2SO_4. Conversely, Mg^{2+}, present at low concentrations in SGW, was not detected in CGW, suggesting its precipitation as insoluble phases ($Mg(OH)_2$) under strongly alkaline conditions (pH > 12.5). The measured pH of CGW exceeded 12.5, reflecting a substantial increase in OH^- concentration owing to OPC dissolution, and thereby reproducing the highly alkaline conditions expected when groundwater is in long-term contact with cementitious materials in repository systems.

ANSI/ANS 16.1 Leaching Test Procedure

The leaching behavior of the geopolymer waste forms was evaluated following the ANSI/ANS 16.1–2003 standard procedure. Although the same leaching data can be applied, differences in interpretation between the 2003 and 2019 versions can cause deviations of approximately ± 0.1–1.0 in the calculated diffusion coefficient (D) and LI. Compared with the 2019 version, the 2003 version includes more leaching intervals, enabling a more detailed analysis of time-dependent behavior. In addition, it generally yields lower LI values, thereby providing a more conservative assessment. Accordingly, this study adopted shortened sampling times based on the ten intervals specified in the 2003 version. Conversely, the calculation of the diffusion coefficients and LI values strictly followed the 2003 interpretation procedure. This approach ensures comparability with previous studies while maintaining distinction from the simplified methodology presented in the 2019 version [48–50].

Semi-dynamic leaching tests were conducted under CGW conditions for 20 d. The leachant-to-specimen surface area ratio was maintained at 10.0 ± 0.1 cm^3/cm^2, and the specimens were immersed in 0.5 L high-density polyethylene containers. The test temperature was maintained at 20 ± 2 °C (18–22 °C).

Leachant replacement and sample collection were performed after 30 s (initial rinse) and subsequently at 1, 2, 4, 6, 13, and 20 d. At each interval, the leachant was completely replaced.

Analytical Methods

Leachate samples were filtered through 0.45 μm membrane filters before analysis. The Cs, Sr, and Co concentrations in the leachate samples were quantified using ICP-MS (Agilent 7850, Agilent Technologies, USA) and ICP-OES (Agilent 5800, Agilent Technologies, USA). The LI was calculated

Table 3 Major ionic composition of SGW and CGW (mg L^{-1})

Leachant type	Na^+	K^+	Ca^{2+}	Mg^{2+}	Cl^-	SO_4^{2-}
SGW	54.1	0.580	8.22	1.74	19.4	8.04
CGW	115	652	1.27×10^3	N.D.	22.1	35.5

according to the ANSI/ANS 16.1 (2003) procedure using the following equation:

$$LI = \frac{1}{n}\sum_{1}^{n}[log\left(\frac{\beta}{D_i}\right)]$$

where LI is the leachability index of the radionuclide, n is the total number of sampling intervals, β is a reference constant (1.0 cm^2/s), and D_i is the effective diffusion coefficient of the radionuclide at the i-th interval (cm^2/s). The effective diffusion coefficient was calculated from the cumulative leached fraction and leaching time.

$$D_i = \pi\left[\frac{a_i}{A_0\,(\Delta\, t)_i}\right]^2\left[\frac{V}{S}\right]^2$$

where a_i is the amount of radionuclide leached during the i-th interval, A_0 is the initial total radionuclide content in the specimen, $(\Delta t)_i$ is the leaching time of the i-th interval (s), and V/S is the ratio of solution volume (cm^3) to specimen surface area (cm^2). In this study, the interval diffusion coefficients were calculated from the cumulative leached fractions, and the resulting LI indicates the long-term radionuclide immobilization performance of the waste forms.

CGW + γ

The long-term performance of geopolymer waste forms under simulated repository conditions was evaluated by simultaneously exposing the specimens to highly alkaline leachant and gamma radiation in a CGW + γ experiment. CGW served as the leachant, and gamma irradiation was provided by a ^{60}Co source with an activity of approximately 1 Ci. The specimens were positioned 46 cm from the source center, corresponding to an average dose rate of approximately 1,308 Gy/d (80.4 Gy/h). The irradiation was performed for 5 d (120 h), yielding a cumulative absorbed dose of approximately 6.36 kGy. This dose level falls within the range reported in previous studies for the early stages of repository gamma fields (several to tens of kGy) and was considered appropriate to simulate structural degradation and accelerated leaching under combined stress conditions. Irradiation parameters were selected to avoid excessive radiolysis and thermal effects, ensuring experimental reproducibility and representativeness of repository conditions [24, 26, 27, 51].

This combined condition simulates an environment where highly alkaline groundwater from cementitious structures chemically degrades the geopolymer matrix, and gamma irradiation simultaneously induces the depolymerization of the aluminosilicate gel network, cleavage of Si–O–Al bonds, and microcrack formation. Consequently, radionuclide leaching can be accelerated compared with single-factor conditions, thereby providing a conservative basis for evaluating the durability of the geopolymer waste forms [24, 51–53]. Under gamma irradiation in CGW, water radiolysis alters the chemical composition of the leachant, including hydrogen gas generation and pH variations. Although primary radicals are short-lived, they readily react with hydroxide or carbonate species in alkaline solutions. In addition, accumulated secondary radiolytic products such as H_2O_2 and $HO_2\cdot$ can also generate small amounts of H^+. These combined reactions slightly reduce the alkalinity of CGW, leading to the observed pH decrease. Such chemical changes may further influence the degradation of the geopolymer matrix and radionuclide release behavior. In the CGW + γ condition, a slight decrease in pH was observed. Although direct experimental reports of pH evolution under this specific combination are scarce, radiolysis studies in cementitious pore solutions have demonstrated that γ-irradiation generates reactive species (·OH, ·H, H_2O_2) even under highly alkaline conditions (pH > 12–13). These species participate in secondary reactions that consume OH^- or carbonate ions, thereby reducing the overall alkalinity of the solution [26, 27, 51, 54–56].

Mechanical and Surface Analysis Methods

Compressive Strength Test

The mechanical integrity of geopolymer waste forms is considered a key indicator for evaluating radionuclide immobilization performance and long-term durability. Therefore, changes in compressive strength before and after leaching tests were measured to verify the structural stability of the specimens. Compressive strength testing was conducted according to ASTM C39 standards using a universal testing machine (UTM; AG-250kNX, Shimadzu Corp., Japan) operated at a constant loading rate of 0.3 MPa/s. The cylindrical specimens were positioned vertically between two parallel compression plates, and the maximum load at failure was recorded. Compressive strength was calculated by dividing the maximum load by the cross-sectional area of the specimen. For each condition, at least two specimens were tested, and the average values were reported.

According to the acceptance criteria established for radioactive waste repositories, cementitious and geopolymer waste forms must achieve a minimum compressive strength of 3.45 MPa (500 psi). The compressive strength evaluation performed in this study directly verifies compliance with these regulatory criteria and provides a basis for assessing the long-term structural stability and disposal suitability of the waste forms.

XPS Analysis

The surface chemical states of the geopolymer waste form specimens were characterized using XPS (K-Alpha, Thermo Fisher Scientific, UK) at the Ulsan National Institute of Science and Technology Central Research Facilities. A monochromatic Al Kα X-ray source was used, with pass energies of 40 eV for high-resolution spectra and 100 eV for survey spectra. The base pressure of the analysis chamber was maintained below 1×10^{-9} mbar. Binding energies were calibrated against the Si 2p peak at 103.0 eV to minimize surface charging effects.

High-resolution spectra of the Cs 3d, Sr 3d, and Co 2p regions were acquired to evaluate changes in the chemical states of the radionuclide surrogates under CGW + γ degradation conditions. Additional spectra of the matrix elements (Si 2p, Al 2p, and O 1s) were also obtained; however, this study focuses on the chemical state variations of Cs, Sr, and Co. Detailed analysis of the matrix elements will be addressed in future work.

All spectra were background-corrected using the Shirley method, and peak deconvolution was performed using Gaussian–Lorentzian line shapes. Spin–orbit splitting values and area ratios were fixed according to literature data, and the full width at half maximum (FWHM) was kept consistent for each chemical species. These procedures ensured reproducibility and enabled a quantitative evaluation of the effects of CGW + γ conditions on the electronic structures and oxidation states of the radionuclide surrogates within the geopolymer matrix.

X-Ray CT Analysis

The internal microstructure and three-dimensional pore distribution of the geopolymer waste forms were characterized using X-ray CT (XTH320LC, Nikon, Japan). Scans were performed at an accelerating voltage of 220 kV and a beam current of 500 μA, using a 2 mm copper filter to minimize beam-hardening effects. A voxel resolution of 10 μm was selected to allow sufficient detection of microcracks and pores.

The raw data were reconstructed using Nikon proprietary reconstruction software, and quantitative image analysis was performed using VGStudio MAX (Volume Graphics GmbH, Germany). Void segmentation was carried out using the Surface Determination module based on gray-value thresholding. Total porosity (ϕ) was calculated as the ratio of segmented void volume (ΣV_{void}) to the total specimen volume (V_{total}) according to the following equation:

$$\phi = \frac{\sum V_{void} \times 100}{V_{total}}$$

Representative pore sizes were obtained using the Defect Analysis module, which reports the equivalent spherical diameter (ESD) for each segmented void. The volume-weighted average pore size was calculated as:

$$d_{avg} = \frac{\sum_{i=1}^{N} d_i V_i}{\sum_{i=1}^{N} V_i}$$

where d_i is the equivalent spherical diameter assigned to void region i, and V_i is its corresponding volume.

Because X-ray CT imaging was performed once per specimen, replicate-based statistical uncertainties could not be directly obtained. Instead, segmentation threshold sensitivity was evaluated by varying the grayscale threshold within a narrow range. This procedure resulted in approximately ± 2–4% variation in the calculated void volume, which is reported as the estimated uncertainty associated with CT-derived porosity and pore-size metrics.

Results and Discussion

Compressive Strength

This section presents compressive strength variations of the geopolymer waste forms. Mechanical stability was evaluated in the pristine state and after leaching under DI, CGW, and CGW + γ conditions to elucidate the effects of different degradation environments on structural integrity.

Table 4 summarizes the compressive strength values for geopolymer waste forms containing Cs, Sr, and Co at concentrations of 1 and 0.1 mmol. Measurements were conducted for the pristine specimens and after leaching under DI, CGW, and CGW + γ conditions.

Table 4 Compressive strength of geopolymer waste forms in the pristine state and after leaching under DI, CGW, and CGW + γ conditions (MPa)

Specimen type	Pristine	After DI	After CGW	After CGW + γ
Cs-0.1 mmol	12.21 ± 0.25	9.43 ± 0.32	6.94 ± 0.57	4.04 ± 0.60
Cs-1 mmol	11.42 ± 0.79	7.34 ± 0.02	5.67 ± 0.58	5.65[a]
Sr-0.1 mmol	14.08 ± 0.24	9.81 ± 0.21	4.56 ± 0.06	2.27[a]
Sr-1 mmol	11.65 ± 1.09	10.36 ± 0.15	9.57 ± 1.75	8.39[a]
Co-0.1 mmol	12.89 ± 2.28	10.86 ± 2.50	6.11 ± 0.17	n/a[b]
Co-1 mmol	15.09 ± 0.19	10.55 ± 0.42	9.83 ± 1.03	7.82 ± 0.63

* [a]: One of the two replicate specimens fractured before testing; compressive strength reported from the remaining intact specimen ($n=1$). Standard deviation not applicable.

* [b]: Both replicate specimens fractured before testing; compressive strength could not be measured (reported as n/a).

The compressive strength of the geopolymer waste forms exhibited distinct variations across different environmental conditions (Figs. 1, 2 and 3).

In the pristine state, all specimens showed compressive strengths ranging from 11 to 15 MPa. The Co-1 mmol (15.09 MPa) and the Sr-0.1 mmol (14.08 MPa) specimens exhibited relatively higher values. This indicates that the aluminosilicate network of the initial geopolymer waste forms was well developed regardless of the radionuclide species or concentration. Overall, the pristine geopolymers demonstrated high initial mechanical stability to conventional cement-based waste forms.

Under DI conditions, the reduction in compressive strength was relatively small. The Cs specimens showed a 20–30% reduction with values ranging from 7.34 to 9.43 MPa, whereas the Sr specimens maintained strengths of 9.81–10.36 MPa, and the Co specimens maintained 10.55–10.86 MPa. These results suggest that structural degradation of the geopolymer network was minimal under simple DI leaching conditions.

Under CGW conditions, a pronounced reduction in compressive strength was observed, indicating degradation of the aluminosilicate network in the highly alkaline environment. The Cs specimens declined to 5.67–6.94 MPa, and the Sr-0.1 mmol specimen showed the greatest reduction, reaching 4.56 MPa. The Co-0.1 mmol specimen decreased

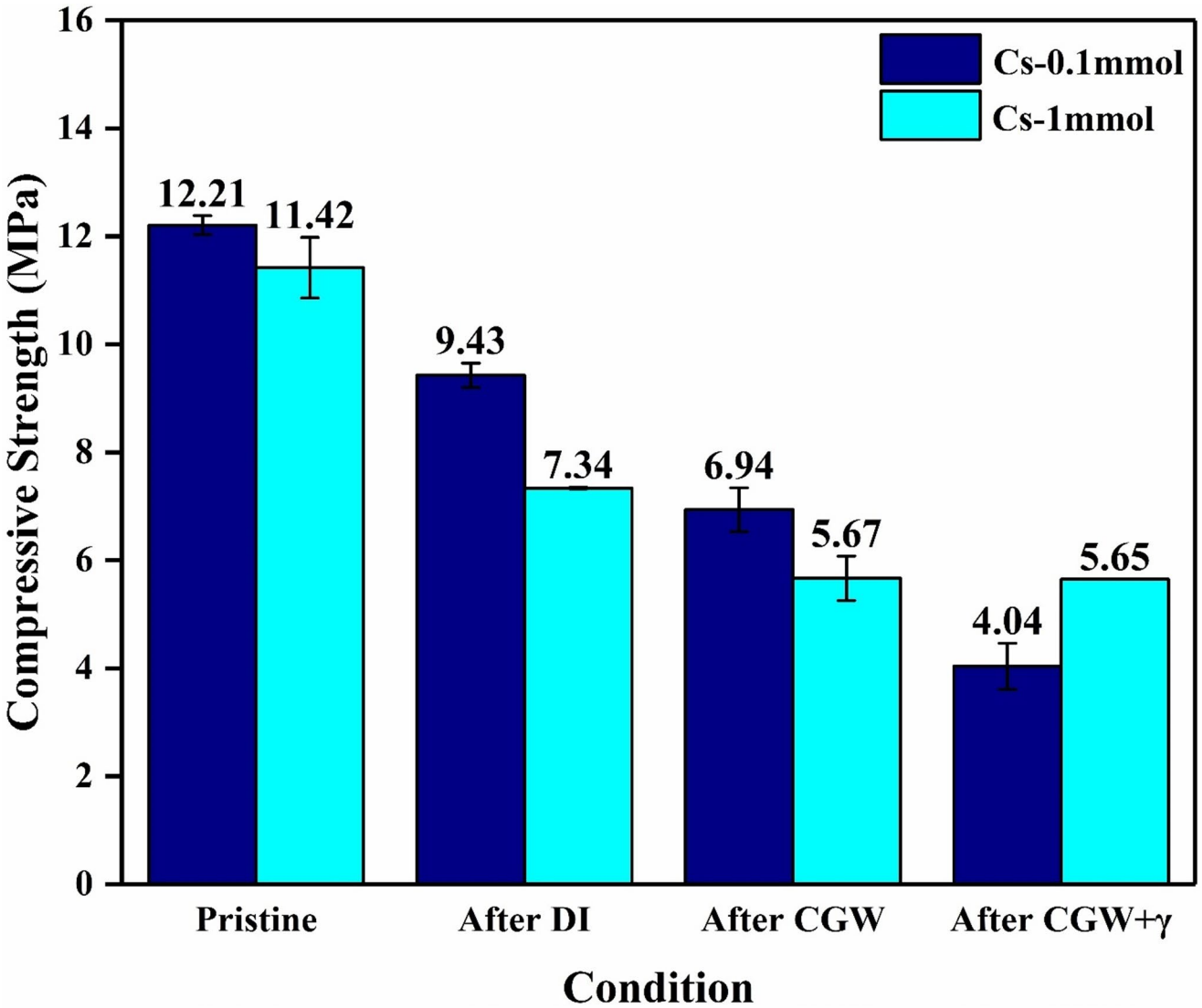

Fig. 1 Compressive strength of Cs-containing geopolymer waste forms (0.1 and 1 mmol) in the pristine state and after leaching under DI, CGW, and CGW+γ conditions. Error bars represent standard deviations ($n=2$), unless otherwise noted

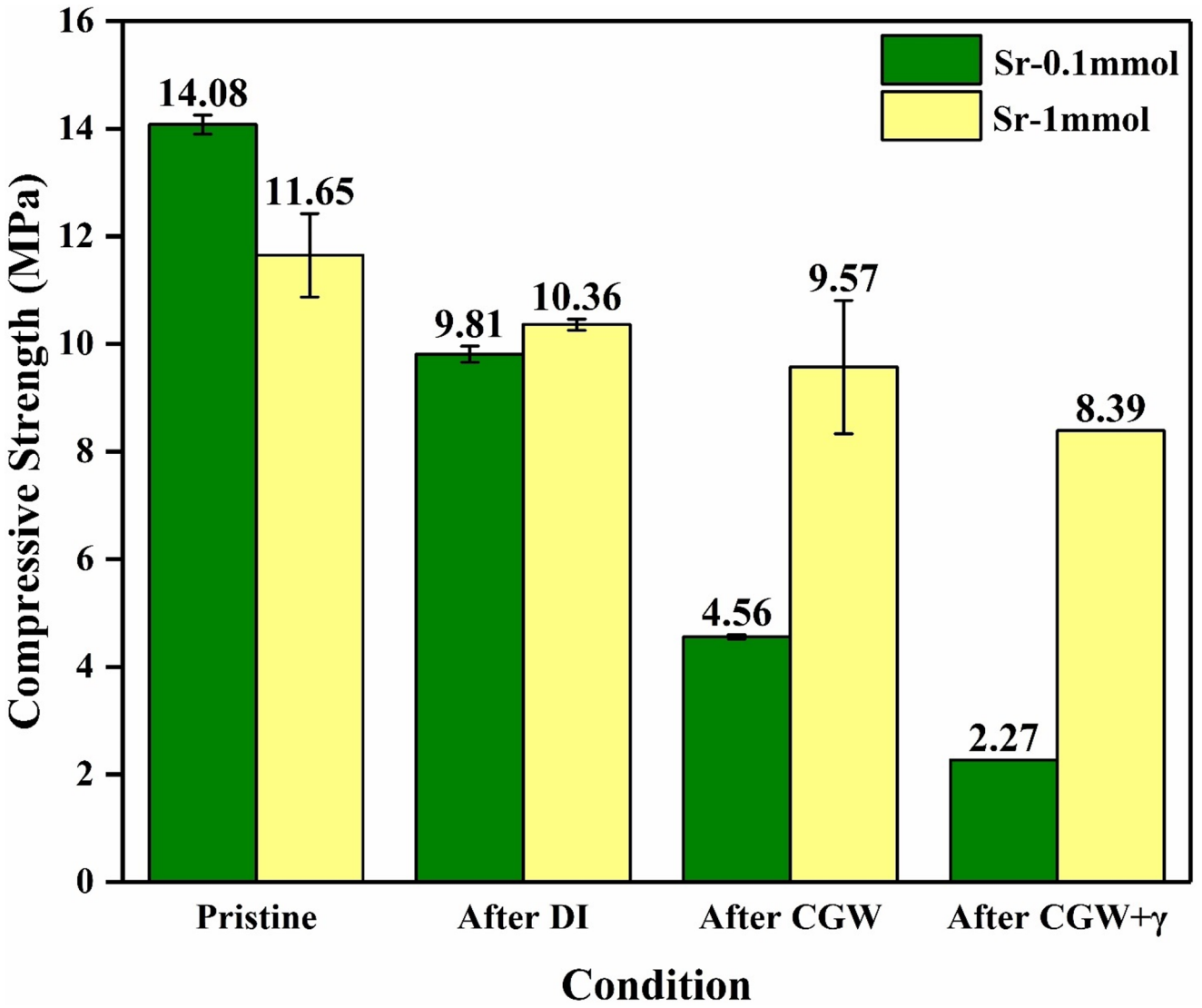

Fig. 2 Compressive strength of Sr-containing geopolymer waste forms (0.1 and 1 mmol) in the pristine state and after leaching under DI, CGW, and CGW + γ conditions. For specimens fractured prior to testing, compressive strength was determined from the remaining intact specimen ($n = 1$)

to 6.11 MPa, corresponding to less than half of its pristine strength. Previous studies have reported that, in highly alkaline environments, alkali attack partially dissolves and reorganizes Si–O–Al and Si–O–Si bonds, thereby inducing microcrack formation and accelerating structural weakening [57–59].

Under CGW + γ conditions, all specimens exhibited a marked reduction in compressive strength. Cs specimens decreased to 4.04–5.65 MPa, while some of the Cs-1 mmol, Sr-0.1 mmol, Sr-1 mmol, and all Co-0.1 mmol specimens fractured before the compressive strength test and could not be measured. For Co-0.1 mmol specimens exposed to CGW + γ conditions, both replicate samples fractured during leaching test and subsequent handling prior to mechanical testing. As a result, compressive strength could not be determined for this condition, indicating severe embrittlement of the geopolymer matrix under combined alkaline and radiolytic stress.

This phenomenon can be attributed to the combined effects of network dissolution in the strongly alkaline solution and radiation-induced chemical reactions. During γ irradiation, water radiolysis generates reactive species such as ·OH, ·H, and H_2O_2, which depolymerize the Si–O–Al network within the geopolymer gel and induce localized chemical changes, thereby exacerbating structural instability. Consistent with this mechanism, the pH of the leachate under CGW + γ conditions decreased from an initial value above 12.55 to 12.1–12.2, whereas no pH change occurred under CGW-only conditions. This decreases supports the local generation of H^+ via radiolysis products and indicates that radiation-induced chemical effects, together with the

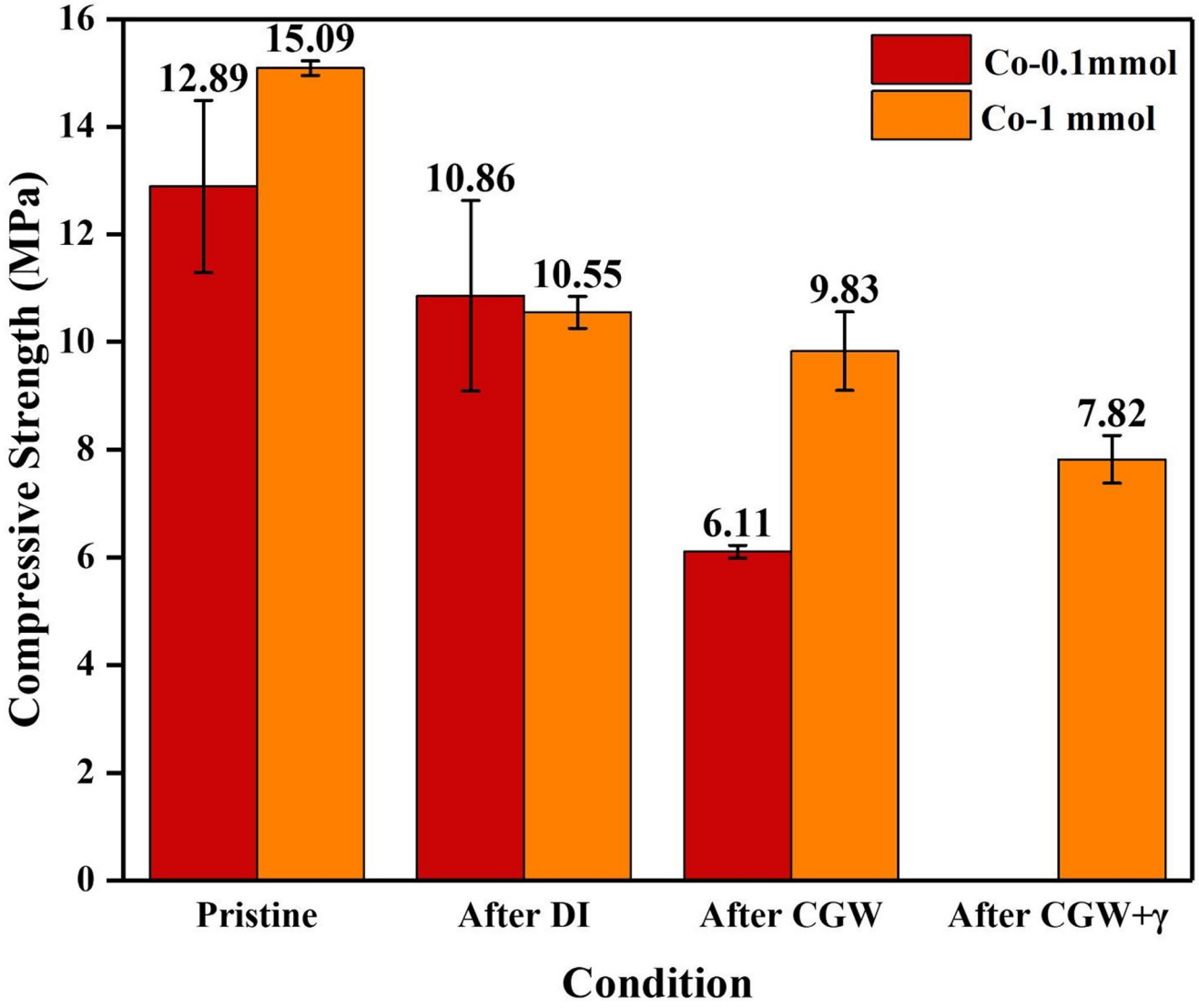

Fig. 3 Compressive strength of Co-containing geopolymer waste forms (0.1 and 1 mmol) in the pristine state and after leaching under DI, CGW, and CGW + γ conditions. For Co-0.1 mmol under CGW + γ conditions, both replicate specimens fractured during immersion and handling prior to testing; therefore, compressive strength could not be measured (reported as n/a)

alkaline environment, accelerated the degradation of the geopolymer waste forms [24, 51–53].

In summary, geopolymer waste forms maintained a certain level of mechanical stability under DI and CGW conditions; however, a pronounced reduction in compressive strength was observed under the CGW + γ conditions, indicating that coupled alkaline and radiolytic effects critically compromise the mechanical integrity of the geopolymer matrix.

Leaching Test

The results of the ANSI/ANS 16.1 leaching tests are summarized in Table 5, which presents the LI values of geopolymer waste forms containing Cs, Sr, and Co under DI, CGW, and CGW + γ conditions. All specimens exhibited LI values above the waste acceptance criterion (LI ≥ 6) defined by ANSI/ANS 16.1, confirming compliance with the regulatory requirement for radionuclide immobilization. This result enables a direct comparison of the radionuclide release behavior under progressively aggressive leaching environments.

Values reported with ± 0.00 indicate that two independent replicate leaching tests yielded identical LI values within the numerical precision of the calculation; therefore, the standard deviation was determined to be zero ($n = 2$).

Under DI conditions, all specimens exhibited high LI values (Cs: 11.3–11.4, Sr: 17.4–17.7, Co: 16.6–16.8), demonstrating stable radionuclide immobilization within the geopolymer matrix. These results are consistent with the

Table 5 LI of geopolymer waste forms under DI, CGW, and CGW+γ conditions

Specimen type	DI	CGW	CGW+γ
Cs-0.1 mmol	11.40±0.28	10.15±0.49	7.90±0.00
Cs-1 mmol	11.30±0.28	10.10±0.28	7.70±0.00
Sr-0.1 mmol	17.65±0.07	8.15±0.35	7.50±0.00
Sr-1 mmol	17.40±0.14	10.25±0.49	9.50±0.00
Co-0.1 mmol	16.55±0.35	14.45±0.35	14.20±0.00
Co-1 mmol	16.75±0.07	16.25±0.35	16.25±0.07

compressive strength data, further confirming that no significant degradation occurred under DI conditions.

Conversely, LI values decreased under CGW conditions, with Sr showing the most significant reduction. The LI of the Sr-0.1 mmol specimen dropped from 17.7 in DI to 8.2 in CGW, whereas Sr-1 mmol decreased from 17.4 to 10.3. This pronounced decrease is attributed to the accelerated leaching of Sr^{2+} via ion exchange with the high concentrations of Ca^{2+} present in CGW, reflecting their similar charge and comparable ionic radii.

Co exhibited a modest decrease in LI under CGW; however, the values remained above 14, indicating relatively stable immobilization. This behavior can be explained by the ability of Co^{2+} to participate in limited electrostatic interactions and ion exchange with the geopolymer gel network, while predominantly forming strong Co–O coordination bonds with –Si–O^- and –Al–O^- sites. Such coordination bonding is significantly more stable than the charge-balancing interactions of Cs^+ or Sr^{2+}, thereby limiting Co leaching even in highly alkaline conditions [60, 61].

Under CGW+γ conditions, the LI values of Cs and Sr decreased further (Cs: 7.7–7.9, Sr: 7.5–9.5), indicating that the combined effects of strong alkalinity and gamma irradiation weakened their leaching resistance. The accelerated release could be attributed to radiation-induced radicals, which destabilized the geopolymer gel network and enhanced radionuclide mobility.

Conversely, Co maintained relatively high LI values (14.2–16.2) even under CGW+γ conditions. Although Co^{3+} is generally capable of forming stronger coordination bonds than Co^{2+}, the relative proportion of Co^{2+} may have increased under irradiation-induced redox perturbations, potentially reducing the overall bonding strength. This explains the slight reduction in LI (by approximately 0.1–0.3). Nevertheless, since Co^{2+} also retains coordination capability with the geopolymer matrix, the overall immobilization capacity was not significantly compromised. These interpretations are consistent with the oxidation-state changes and bonding characteristics revealed in the subsequent XPS analysis (Sect. 3.4).

Notably, under the same CGW+γ conditions, the compressive strength was markedly reduced, whereas the LI of Co remained above 14. This contrast suggests that mechanical degradation and chemical immobilization capacity do not necessarily evolve in a coupled manner. The sustained chemical stability of Co suggests that coordination bonding, characteristic of transition metals, plays a critical role in maintaining immobilization despite mechanical damage to the matrix.

In summary, Cs and Sr exhibited pronounced sensitivity to combined alkaline and irradiation conditions, resulting in decreased leaching resistance, while Co maintained stable LI values across all conditions. The leaching results confirmed that cumulative radionuclide release increased under CGW+γ, consistent with the compressive strength results and confirming that structural degradation of the waste form translates into diminished immobilization performance. To further elucidate the structural origins of these leaching trends, CT analysis was conducted to investigate changes in the internal microstructure.

Collectively, the leaching behavior aligns strongly with the mechanical degradation trends reported in Sect. 3.1 and the microstructural changes observed in Sect. 3.3. The substantial LI reductions of Cs and Sr under CGW+γ correspond to the severe strength losses and porosity growth, indicating that depolymerization of the Si–O–Al framework directly enhances radionuclide mobility. In contrast, the consistently high LI of Co, despite mechanical weakening, demonstrates that coordination bonding can remain chemically robust even when the bulk structure deteriorates. As further validated by XPS in Sect. 3.4, element-specific changes in electron density and bonding environments provide the molecular-scale origin of these differences. These integrated results establish a unified degradation mechanism in which alkaline dissolution, ion exchange, radiation-induced bond cleavage, and surface chemical restructuring collectively govern radionuclide release under multi-stressor conditions.

X-Ray CT Analysis

The internal pore structure of the geopolymer waste forms was quantitatively characterized using X-ray CT. The porosity values obtained under different conditions are summarized in Table 6.

The initial porosity of the specimens ranged from 0.5 to 2.8%, depending on the type and concentration of the

Table 6 Porosity (%) of geopolymer waste forms in the pristine state and after leaching under DI, CGW, and CGW+γ conditions

Specimen type	Pristine	DI	CGW	CGW+γ
Cs-0.1 mmol	1.14	0.73	0.71	4.20
Cs-1 mmol	2.49	0.93	1.80	3.18
Sr-0.1 mmol	1.82	0.70	1.30	3.61
Sr-1 mmol	1.24	1.02	0.88	4.58
Co-0.1 mmol	2.79	1.59	2.03	1.15
Co-1 mmol	0.49	0.39	0.26	2.44

Note: CT parameters represent single measurements. Estimated uncertainty (±2–4% relative) was evaluated based on segmentation threshold sensitivity

Table 7 Representative maximum void sizes (mm^3) of geopolymer waste forms in the pristine state and after leaching under DI, CGW, and CGW+γ conditions

Specimen type	Pristine	DI	CGW	CGW+γ
Cs-0.1 mmol	~0.60	~0.15	~0.18	~1.00
Cs-1 mmol	~1.40	~0.18	~0.40	~1.40
Sr-0.1 mmol	~1.30	~0.58	~1.30	~2.40
Sr-1 mmol	~0.18	~0.19	~0.01	~7.80
Co-0.1 mmol	~0.40	~0.27	~0.45	~1.30
Co-1 mmol	~0.12	~0.08	~0.06	~1.40

radionuclide surrogate. Under DI and CGW conditions, porosity changes were minimal in most cases, confirming that leaching alone caused limited structural degradation [62].

However, all specimens exhibited a pronounced increase in porosity under CGW + γ conditions. This can be attributed to the combined effects of alkali-induced network dissolution and radiolytic damage, which collectively facilitated microcrack formation and pore enlargement [54]. Cs- and Sr-containing specimens showed porosity levels of approximately 3–4%, indicating significant structural degradation. For the Co-containing specimens, relatively large fluctuations in porosity were observed across the different test conditions. These variations do not indicate fundamentally different degradation behavior, but rather reflect specimen-to-specimen variability inherent to geopolymer materials, as discussed below.

According to the pore size distribution analysis (Table 7), most pores were confined to small voids smaller than 1.4 mm^3 under the pristine, DI, and CGW conditions. However, under CGW+γ conditions, new large pores (>1.0 mm^3) were detected in all radionuclide-containing specimens. The Sr-1 mmol specimen, which initially contained only small pores of approximately 0.18 mm^3, exhibited large pores up to 7.8 mm^3 after CGW+γ exposure, indicating the most severe degradation. Similarly, the Cs-1 mmol specimen initially displayed relatively large pores (~1.4 mm^3) in the pristine state, while the CGW+γ condition also induced the appearance of large pores (>1.0 mm^3) in the Cs-0.1 mmol specimen. Although the Co-containing specimens initially exhibited the smallest pore sizes among all radionuclides, new large pores exceeding 1.0 mm^3 were generated under CGW+γ, confirming microcrack propagation and structural degradation.

While the maximum pore sizes were similar in some specimens between the pristine and CGW+γ conditions, the increased frequency of abundance of large-pore features under CGW+γ indicate that microvoids coalesced and propagated into cracks, which subsequently evolved into large pores through repeated growth. Therefore, both total porosity and the emergence of large pores serve as critical indicators of radiation-assisted degradation in MK-based geopolymers.

Such internal structural degradation was also evident on the specimen surfaces. No noticeable surface changes were observed under DI conditions, whereas white precipitates formed under CGW conditions and increased markedly under CGW+γ conditions. X-ray diffraction analysis identified these precipitates as $CaCO_3$. Since MK-based geopolymers are inherently Ca-free (<0.04 wt%), the $CaCO_3$ likely originated from the CGW leachant, which contains a high Ca^{2+} concentration (1.27×10^3 mg/L). The formation of $CaCO_3$ under CGW can be explained by the natural precipitation of Ca^{2+} in a highly alkaline environment (pH>12.5), where CO_3^{2-} species dominate.

However, the markedly greater $CaCO_3$ deposition under CGW + γ cannot be attributed solely to solution chemistry; rather, it is interpreted as a consequence of irradiation-enhanced surface reactivity and defect formation. The radiolytic process generates reactive radicals that create microcracks and defects on the geopolymer surface, which in turn promote the adsorption and precipitation of Ca^{2+} and CO_3^{2-}. Thus, increased $CaCO_3$ deposition should be viewed as an indicator of radiation-assisted surface degradation,

rather than as a densifying mechanism, further supporting the proposed degradation mechanism under combined conditions [63].

Overall, the CT analysis results were consistent with the previously observed reductions in compressive strength and LI, providing qualitative and quantitative evidence that the CGW + γ condition compromises the structural stability of the geopolymer matrix. The small variability observed among specimens with similar compositions is attributed to intrinsic microstructural heterogeneity rather than to systematic differences in degradation mechanisms.

Alkali-activated geopolymers are inherently heterogeneous materials, owing to the coexistence of partially dissolved metakaolin particles, uneven gel formation, and inevitable mixing-related variability. In the present study, heterogeneity was further influenced by the presence of metal cations (Cs^+, Sr^{2+}, Co^{2+}), whose dispersion within the fresh paste may not be perfectly uniform, thereby locally affecting the dissolution kinetics of metakaolin and the polycondensation rate of the aluminosilicate gel. As a result, nominally identical specimens exhibited differences in pore connectivity, microcrack distribution, and matrix density. Under CGW + γ conditions, γ-induced depolymerization and localized radiolytic weakening amplify these pre-existing microstructural differences, contributing to the observed specimen-to-specimen variability in CT-derived porosity, compressive strength, and radionuclide leaching.

XPS Analysis

Several previous studies have reported radiation-induced pH modification in alkaline cementitious and aluminosilicate systems, attributed to the production of radiolytic species such as H^+, H_2O_2, and reactive radicals during water radiolysis. In cement pore solutions and alkali-activated matrices, γ irradiation has been shown to induce local acidification despite high initial pH, supporting the pH decrease observed under CGW + γ conditions in this study. High-resolution XPS analysis was conducted to investigate the chemical mechanisms responsible for the reductions in compressive strength and the accelerated leaching behavior observed under the CGW + γ condition [27, 64, 65].

Under this condition, all specimens exhibited a pronounced increase in the intensities of the Cs 3d, Sr 3d, and Co 2p peaks. This behavior indicates that depolymerization of the geopolymer gel network and surface degradation exposed radionuclides previously immobilized within the matrix. This spectral enhancement is consistent with the ion-migration behavior inferred from the leaching results, demonstrating that structural breakdown promotes transport of charge-balancing cations toward the surface.

The concurrent increase in peak intensity across all radionuclides indicates that the aluminosilicate framework underwent significant depolymerization, exposing charge-balancing sites (-Si-O^-, -Al-O^-) and promoting cation migration toward the surface. However, the direction and magnitude of the binding-energy (BE) shifts differ among Cs, Sr, and Co, reflecting their distinct bonding characteristics and immobilization mechanisms within the geopolymer matrix.

As shown in Fig. 4, the Cs 3d spectrum comprises a $3d_{5/2}$ (~725 eV) and $3d_{3/2}$ (~740 eV) doublet. Under the CGW + γ condition, the intensity increased by more than 1000 cps compared with the pristine specimen, accompanied by a low-BE shift of approximately 0.4 eV.

This shift suggests that Cs^+, weakly adsorbed electrostatically onto negatively charged -Si-O^- sites, migrated toward regions with higher local electron density created by network depolymerization. The relaxation of the Cs–O environment and redistribution of surface charge lower the observed BE, indicating that Cs remains primarily surface-bound rather than structurally incorporated [66]. This spectroscopic signature aligns with the pronounced decrease in LI, confirming that Cs is immobilized mainly through weak outer-sphere interactions that deteriorate rapidly under alkaline and irradiation conditions.

As shown in Fig. 5, the Sr 3d spectrum exhibits peaks at $3d_{5/2}$ (133.4 eV) and $3d_{3/2}$ (135.2 eV) in the pristine specimen. Under the CGW + γ condition, these peaks shifted to 134.2 and 136.0 eV, respectively, corresponding to a high-BE shift of approximately 0.8 eV.

The high-BE shift can be attributed to partial substitution of Sr^{2+} by Ca^{2+} from CGW and the subsequent decrease in electron density around Sr-O coordination sites. Although Sr forms relatively strong ionic bonds with the Si-O-M-O-Al (M = Ca, Sr) framework, the alkali-induced dissolution and cation exchange process disrupt these linkages, producing Sr-enriched surface species such as Sr-OH or Sr-O. The reduced electron density in these species accounts for the high-BE shift.

The simultaneous increase in intensity confirms surface accumulation of Sr through dissolution-reprecipitation and ion-exchange mechanisms [67–70]. Unlike Cs^+ and Co^{2+}, whose bonding environments become electronically relaxed upon network depolymerization, Sr^{2+} experiences electron-density depletion due to competitive Ca^{2+}–Sr^{2+} ion exchange and formation of oxygen-coordinated Sr–O(H) surface species. This fundamental difference in the chemical response of Sr explains why only Sr exhibits a high-BE shift, whereas Cs and Co shift toward lower BE.

As shown in Fig. 6, the Co 2p spectrum reveals contributions from Co^{2+} and Co^{3+} species. In the pristine specimen, the Co^{2+} $2p_{3/2}$ and Co^{3+} $2p_{3/2}$ peaks appeared at 780.4 and

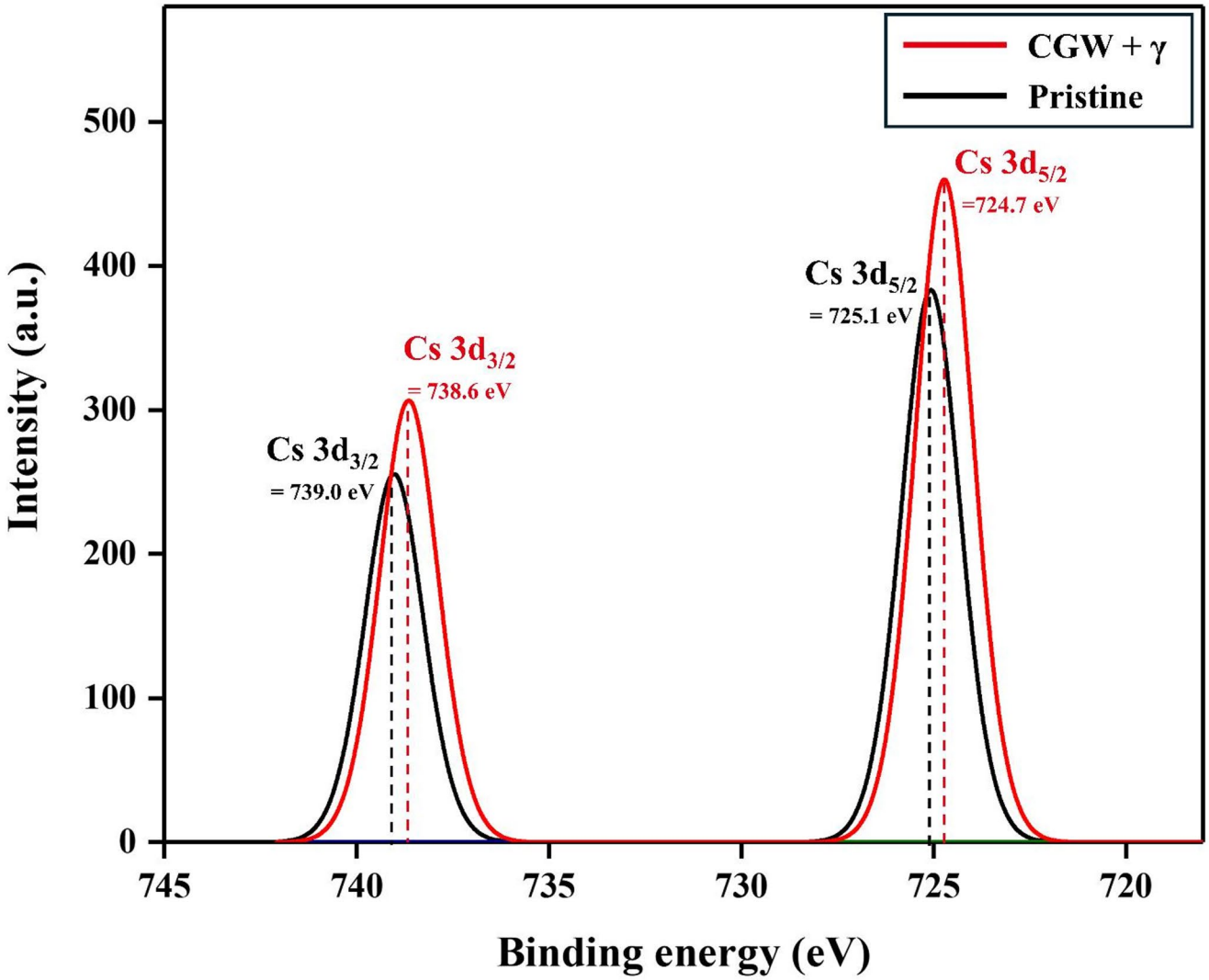

Fig. 4 Comparison of the Cs 3d XPS spectra between the pristine geopolymer and CGW+γ degraded specimen

781.4 eV, respectively, while under the CGW+γ condition, these peaks shifted to 780.7 and 781.7 eV. Likewise, in the $2p_{1/2}$ region, the Co^{2+} (795.4 eV) and Co^{3+} (796.4 eV) peaks shifted to 795.7 and 796.7 eV, respectively. Quantitative fitting showed that the Co^{2+} fraction increased markedly from 42.86 to 71.73%, indicating partial reduction of Co^{3+} to Co^{2+}.

Although reduction typically lowers BE by increasing the local electron density, the opposite trend—a net high-BE shift of approximately 0.3 eV—indicates that alterations in the coordination environment dominate over the valence effect. Under CGW + γ, radiolysis-assisted depolymerization and oxygen-vacancy formation displaced Co species from well-coordinated aluminosilicate sites into defect-rich, lower-coordination surface sites with more asymmetric electrostatic fields, which increased BE despite the concurrent Co^{3+} to Co^{2+} reduction. The overall intensity increase further confirms Co migration from the bulk to the surface. Collectively, the intensity gain, oxidation-state redistribution, and net high-BE shift provide direct spectroscopic evidence that coordination-environment changes and surface defect formation govern the radiation-enhanced chemical destabilization of the geopolymer matrix under CGW + γ conditions [71–73].

These spectroscopic trends are fully consistent with the macroscopic degradation behavior described in Sect. 3.2 and 3.3. The low-BE shift and intensity increase of Cs correspond directly to its sharply reduced LI, confirming that the weakening of Cs–O interactions observed by XPS translates into enhanced macroscopic mobility. Similarly, the high-BE shift of Sr aligns with the severe decline in LI caused by Ca–Sr exchange in CGW, indicating that electron-density depletion at Sr sites reflects the same ion-exchange-driven destabilization observed in the leaching tests. In contrast,

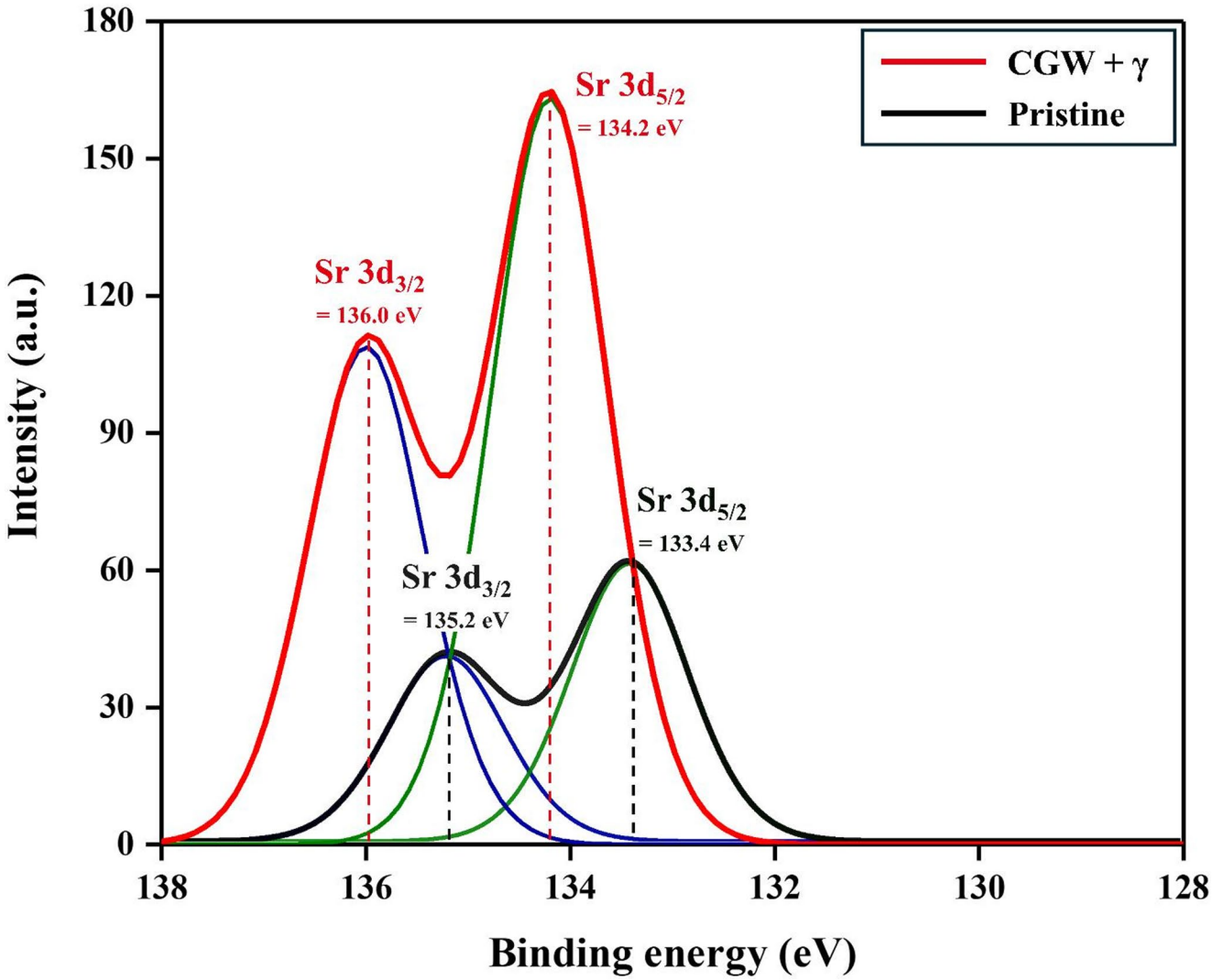

Fig. 5 Comparison of the Sr 3d XPS spectra between the pristine geopolymer and CGW + γ degraded specimen

Co shows only a minor reduction in LI, and XPS reveals that Co retains inner-sphere coordination even under CGW + γ conditions. These correlations demonstrate that the BE shifts provide a direct chemical explanation for the element-specific leaching behavior and validate the degradation mechanisms inferred from the previous observations.

Overall, the compressive strength, leachability, CT, and XPS results collectively reveal a unified degradation behavior of geopolymer waste forms under CGW + γ conditions. The pronounced loss of mechanical integrity reflects the synergistic effects of alkaline dissolution and radiation-induced depolymerization of the aluminosilicate network. These chemical and structural alterations manifest at the microstructural scale as increased porosity and structural heterogeneity, as confirmed by CT analysis, which in turn facilitate enhanced transport pathways for radionuclides and contribute to the reduced leachability index observed for Cs and Sr.

At the molecular scale, XPS analysis demonstrates that radiolysis not only accelerates bulk structural degradation but also induces element-specific modifications in bonding environment and electron density at the geopolymer surface. These electronic and chemical changes provide a mechanistic basis for the observed macroscopic performance degradation. Taken together, the results indicate that mechanical weakening, microstructural evolution, and radionuclide destabilization are intrinsically linked responses to coupled alkaline and radiolytic stress, underscoring the importance of integrated, multi-scale evaluation for long-term disposal safety.

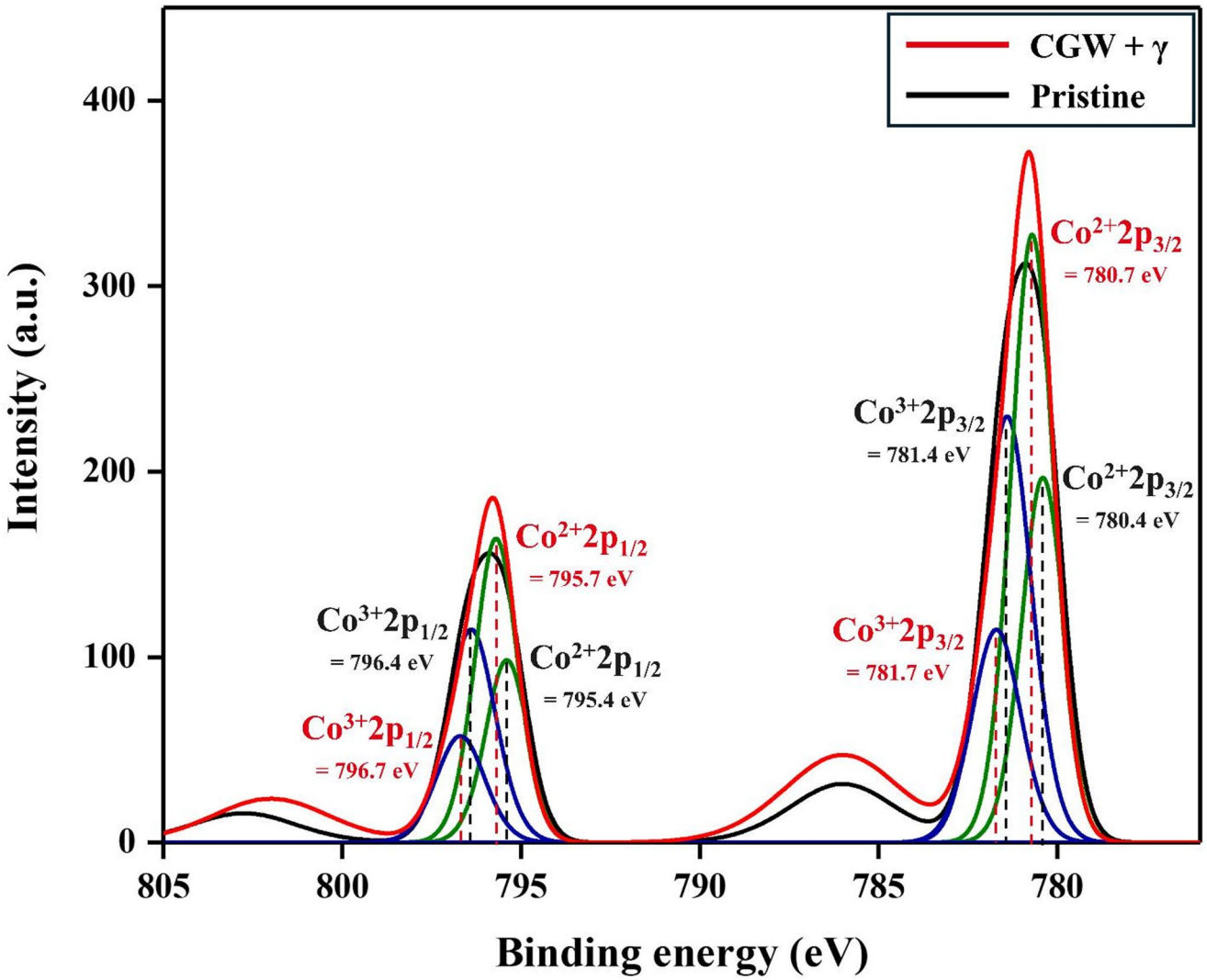

Fig. 6 Comparison of the Co 2p XPS spectra between the pristine geopolymer and CGW + γ degraded specimen

Conclusion

In this study, the long-term integrity of MK-based geopolymer waste forms was evaluated under simulated repository conditions. Specimens exhibited stable mechanical and chemical performance under DI conditions; in contrast, exposure to CGW caused strength loss and reduced leachability owing to hydroxide-induced depolymerization of aluminosilicate bonds. The CGW + γ condition produced the most severe degradation, evidenced by mechanical weakening, accelerated leaching of Sr and Cs, increased porosity observed by CT analysis, and surface enrichment and oxidation state changes identified by XPS.

The synergistic effects of the alkaline environment and γ irradiation caused structural and chemical deterioration of geopolymer waste forms. Hydroxide ions (OH^-) disrupted Si–O–Al bonding, and radiolytic species generated from water promoted oxygen-vacancy formation, facilitating microcrack propagation and charge redistribution within the geopolymer matrix. XPS analysis confirmed that Cs migrated toward negatively charged surface sites via weak electrostatic bonding, Sr experienced electron depletion from Ca–Sr ion exchange, and Co underwent partial reduction from Co^{3+} to Co^{2+}, accompanied by coordination asymmetry and net binding-energy shifts. These results demonstrate that combined alkaline and radiolytic stresses alter the oxidation state and coordination environment of immobilized cations, accelerating overall degradation.

While the specimens retained integrity under single-factor conditions, their performance deteriorated markedly under the coupled CGW + γ condition. Therefore, durability evaluations of geopolymer waste forms should incorporate multi-factor environmental conditions that reflect realistic repository scenarios to establish reliable long-term performance boundaries. This study provides mechanistic insights

into the coupled degradation processes of geopolymer waste forms and establishes a conservative dataset for repository safety evaluations.

Acknowledgements This work was supported by Korea Hydro & Nuclear Power Co., Ltd. (No. 2023-Tech-14).
This work was supported by the Nuclear Safety Research Program through the Korea Foundation of Nuclear Safety (KoFONS) using the financial resource granted by the Nuclear Safety and Security Commission (NSSC) of the Republic of Korea. (RS-2025-02311585)
The authors acknowledge the use of facilities and technical assistance provided by the UNIST Central Research Facilities (UCRF).

Author contributions Conceptualization: S. Kwon; Methodology: S. Kwon; Data collection and analysis: S. Kwon, Y. Lee, Y. Oh; Writing – original draft: S. Kwon; Writing – review and editing: S. Kwon, Y. Lee, Y. Oh, J. Park; Supervision: J. Park.

Funding Open Access funding enabled and organized by Ulsan National Institute of Science and Technology (UNIST)

Declarations

Competing Interests The authors declare that they have no known competing financial interests or personal relationships that could have appeared to influence the work reported in this paper.

References

1. J.L. Provis, J.S.J. van Deventer, Geopolymers, Woodhead Publ. Ltd., Cambridge (2009)
2. M.I. Ojovan, W.E. Lee, S.N. Kalmykov, *An Introduction To Nuclear Waste Immobilisation* (Elsevier, Amsterdam, 2019)
3. A. Fernández-Jiménez, A. Palomo, M. Criado, Cem. Concr Res. **35**, 1204 (2005)
4. K. Komnitsas, D. Zaharaki, Min. Eng. **20**, 1261 (2007)
5. J.L. Provis, G.C. Lukey, J.S.J. van Deventer, Chem. Mater. **17**, 3075 (2005)
6. H. Xu, J.S.J. van Deventer, Int. J. Min. Process. **59**, 247 (2000)
7. J.L. Provis, S.A. Bernal, Annu. Rev. Mater. Res. **44**, 299 (2014)
8. R.R. Lloyd, J.L. Provis, J.S.J. van Deventer, J. Mater. Sci. **44**, 620 (2009)
9. I. Tsuneki, W. Sadayuki, A. Hiroyuki, H. Kazuko, Y. Kazuo, J. Soc. Remed Radioact Contam. Environ. **8**, 1 (2020)
10. E. Mukiza, Q.T. Phung, L. Frederickx, D. Jacques, S. Seetharam, G. De Schutter, J. Nucl. Mater. **585**, 154639 (2023)
11. F. Pacheco-Torgal, J. Castro-Gomes, S. Jalali, Constr. Build. Mater. **22**, 1315 (2008)
12. C.A. Rees, J.L. Provis, G.C. Lukey, J.S.J. van Deventer, Colloids Surf. Physicochem Eng. Asp. **318**, 97 (2008)
13. P. Duxson, J.L. Provis, G.C. Lukey, J.S.J. van Deventer, Cem. Concr Res. **37**, 1590 (2007)
14. A.M. Rashad, Constr. Build. Mater. **41**, 303 (2013)
15. K. Komnitsas, D. Zaharaki, G. Bartzas, Appl. Clay Sci. **73**, 103 (2013)
16. Z. Yunsheng, S. Wei, C. Qianli, C. Lin, J. Hazard. Mater. **143**, 206 (2007)
17. L. Zheng, W. Wang, Y. Shi, Chemosphere. **79**, 665 (2010)
18. B.I. El-Eswed, R.I. Yousef, M. Alshaaer, I. Hamadneh, S.I. Al-Gharabli, F. Khalili, Int. J. Min. Process. **137**, 34 (2015)
19. J. Fan, J. Yan, M. Zhou, Y. Xu, Y. Lu, P. Duan, Y. Zhu, Z. Zhang, W. Li, A. Wang, D. Sun, J. Hazard. Mater. **453**, 131380 (2023)
20. Q. Zhang, Y. Jiang, X. Zhao, J. Chen, D. Xia, B. Zhang, J. Duan, Front. Mater. **9**, 929639 (2022)
21. F. Yokaichiya, E.A.G. Ferreira, R. Vicente, A. Cerceau, J.T. Marumo and, Franco, Nucl. Instrum. Methods Phys. Res. B **546**, 165160 (2024). M. K. K. D
22. A. Mutoni, J. Kim, Appl. Sci. **12**, 89009 (2022)
23. E.B.A. Moyce, C. Rochelle, K. Morris, A.E. Milodowski, X. Chen, S. Thornton, J.S. Small, S. Shaw, Appl. Geochem. **50**, 91 (2014)
24. N. Deng, H. An, H. Cui, Y. Pan, B. Wang, L. Mao, J. Zhai, J. Nucl. Mater. **459**, 270 (2015)
25. M. Houhou, N. Leklou, H. Ranaivomanana, J.D. Penot, S. de Barros, Discov Appl. Sci. **7**, 126 (2025)
26. D.A. Geddes, B. Walkley, C.L. Le Galliard, M. Hayes, S.A. Bernal, J.L. Provis, J. Am. Ceram. Soc. **107**, 4621 (2024)
27. D. Lambertin, C. Boher, A. Dannoux-Papin, K. Galliez, A. Rooses, F. Frizon, J. Nucl. Mater. **443**, 311 (2013)
28. M.L.Y. Yeoh, T. Wang, P. Leong, C.T. Chen, D.L. Chen, J. Hazard. Mater. **407**, 124805 (2021)
29. J.G. Jang, S.M. Park, H.K. Lee, J. Hazard. Mater. **318**, 339 (2016)
30. L. Frederickx, E. Mukiza, Q.T. Phung, Sustainability. **17**, 41756 (2025)
31. D.C. Tompkins, D.I. Stewart, J.T. Graham, I.T. Burke, J. Hazard. Mater. Adv. **5**, 100043 (2022)
32. J. Xing, L. Gao, Z. Zhang, N. Luo, Alex Eng. J. **107**, 468 (2024)
33. Y. Reches, Results Mater. **2**, 100039 (2019)
34. E.O. Echeweozo, S. Alomairy, N.S. Alsaiari, M.S. Al-Buriahi, Sci. Rep. **14**, 29968 (2024)
35. B. Mast, M.K. Nguyen, J.R. Smith, D.A. Baldwin, W.P. Gates, J. Nucl. Mater. **539**, 152237 (2020)
36. J.I.T. Garces, A.A.S. Tigue, M.A.B. Promentilla, Chem. Eng. Trans. **94**, 224 (2022)
37. J.G.S. Van Jaarsveld, J.S.J. Van Deventer, L. Lorenzen, Min. Eng. **10**, 659 (1997)
38. P. Sekely, M. Valica, S. Sekely, M. Horník, Sci. Technol. **135**, 13 (2023)
39. M.Y. Khalil, E. Merz, J. Nucl. Mater. **211**, 141 (1994)
40. A. Fernández-Jiménez, A. Palomo, Fuel. **82**, 2259 (2003)
41. Z. Sun, A. Vollpracht, Cem. Concr Res. **136**, 106161 (2020)
42. K.C. Onyelowe, F.E. Ikeagwuani, P.J. Nwachukwu, C.C. Ugwu, Sci. Rep. **13**, 18901 (2023)
43. R.P. Williams, A. Van Riessen, Fuel. **89**, 3683 (2010)
44. J. Ahn, W.S. Kim, W. Um, J. Nucl. Mater. **518**, 247 (2019)
45. R.A. Sa Ribeiro, M.G. Sa Ribeiro, D.M. Samuel, A. Ozer, P. Numkiatsakul, W.M. Kriven, Mater. Struct. **58**, 142 (2025)
46. J. Kohout, P. Koutník, P. Hájková, E. Kohoutová, A. Soukup, Polymers. **13**, 3754 (2021)

47. H. Byeon, Y. Lee, S. Kwon, Y. Oh, J. Park, Prog Nucl. Energy. **190**, 105978 (2026)
48. A.N. Society, *Measurement of the Leachability of Solidified Low-Level Radioactive Wastes by a Short-Term Test Procedure, ANSI/ANS-16.1* (American Nuclear Society, Illinois, 2003)
49. American Nuclear Society, *Measurement of the Leachability of Solidified Low-Level Radioactive Wastes by a Short-Term Test Procedure, ANSI/ANS-16.1* (American Nuclear Society, Illinois, 2019)
50. Y. Shin, B. Kim, J. Kang, H.M. Ma, W. Um, Nucl. Eng. Technol. **55**, 3617 (2023)
51. V. Cantarel, M. Arisaka, I. Yamagishi, J. Am. Ceram. Soc. **102**, 7553 (2019)
52. E. Mukiza, L. Frederickx, Q.T. Phung, D. Jacques, G. De Schutter, J. Nucl. Mater. **614**, 155912 (2025)
53. M.S. Eid, I.I. Bondouk, H.M. Saleh, K.M. Omar, H.M. Diab, Sustainability. **15**, 10763 (2023)
54. O. Roth, J.A. Laverne, J. Phys. Chem. A **115**, 700 (2011)
55. S. Le Caër, L. Dezerald, K. Boukari, M. Lainé, S. Taupin, R.M. Kavanagh, A. Saúl, Cem. Concr Res. **100**, 110 (2017)
56. P. Bouniol, J. Nucl. Mater. **403**, 167 (2010)
57. K. Oliwa, B. Kozub, K. Łoś, P. Łoś, K. Korniejenko, Mater. (Basel). **18**, 3892 (2025)
58. I. Ismail, S.A. Bernal, J.L. Provis, S. Hamdan, J.S.J. van Deventer, Mater. Struct. **46**, 361 (2013)
59. N. Ukrainczyk, O. Vogt, RILEM Tech. Lett. **5**, 163 (2020)
60. Q. Yu, S. Han, W. Wang, T. Zhang, G. Li, J. Clean. Prod. **234**, 97 (2019)
61. J. Park, S. Cho, H. Suh, S. Her, J. Yang, S. Bae, Cem. Concr Res. **195**, 107921 (2025)
62. S. Wang, L. Yu, L. Xu, K. Wu, Z. Yang, Mater. (Basel). **14**, 5299 (2021)
63. M.A. Longhi, Z. Zhang, E.D. Rodríguez, A.P. Kirchheim, H. Wang, Front. Mater. **6**, 89 (2019)
64. J. Wen, X. Liu, D. Zhang, Y. Hu, Z. Zhao, C. Chen, J. Am. Ceram. Soc. **108**, 70160 (2025)
65. M.E. Simonsen, C. Sønderby, Z. Li, E.G. Søgaard, J. Mater. Sci. **44**, 2079 (2009)
66. X. Niu, Y. Elakneswaran, C.R. Islam, J.L. Provis, T. Sato, J. Hazard. Mater. **429**, 128373 (2022)
67. L.B. Wang, Y.S. Li, X. Zhao, T. Zhang, Physica C, **282**, 989–990 (1997)
68. Y.H. Huang, Y.C. Wu, Polymers. **14**, 992 (2022)
69. H. Türk, A. Becker, M. Kruse, J. Li, ChemCatChem. **14**, 300 (2022)
70. S. Lizzit, A. Baraldi, P. Hofmann, A. Plummer, R. Larciprete, Phys. Rev. B **63**, 205419 (2001)
71. C. Huang, M. Chen, L. Wang, J. Xu, F. Zhao, Q. Liu, Waste Dispos. Sustain. Energy. **7**, 353 (2025)
72. Q. Lian, P.D. Thesis, ProQuest LLC, Michigan (2021)
73. X. Xu, H. Liu, H. Bi, S. Wang, P. Zhao, Y. Huang, X. Cheng, Constr. Build. Mater. **261**, 120013 (2020)